Constraints on the synchronization of entorhinal cortex stellate cells

Patrick Crotty* and Eric Lasker
Department of Physics and Astronomy, Colgate University, 13 Oak Drive, Hamilton, New York 13346, USA

Sen Cheng
Mercator Research Group "Structure of Memory," Fakultät für Psychologie, Ruhr-Universität, 44801 Bochum, Germany
(Received 9 April 2012; revised manuscript received 22 June 2012; published 10 July 2012)

Synchronized oscillations of large numbers of central neurons are believed to be important for a wide variety of cognitive functions, including long-term memory recall and spatial navigation. It is therefore plausible that evolution has optimized the biophysical properties of central neurons in some way for synchronized oscillations to occur. Here, we use computational models to investigate the relationships between the presumably genetically determined parameters of stellate cells in layer II of the entorhinal cortex and the ability of coupled populations of these cells to synchronize their intrinsic oscillations: in particular, we calculate the time it takes circuits of two or three cells with initially randomly distributed phases to synchronize their oscillations to within one action potential width, and the metabolic energy they consume in doing so. For recurrent circuit topologies, we find that parameters giving low intrinsic firing frequencies close to those actually observed are strongly advantageous for both synchronization time and metabolic energy consumption.

DOI: 10.1103/PhysRevE.86.011908 PACS number(s): 87.19.lb, 87.19.ll, 87.19.lo, 02.60.Pn

I. INTRODUCTION

The synchronized activity of large numbers of neurons is a common phenomenon in mammalian brains. Such activity is a stereotypical feature of electroencephalography (EEG) and local field potential (LFP) recordings, in which certain frequency ranges are strongly dominant depending on the brain region, wakefulness state, and current behavior of the animal. While much about the functional role and behavioral correlates of large-scale neural synchrony remains speculative or unknown [1], there is increasing agreement that it plays an important role in information processing and coding.

Recently, the θ rhythm (approximately 8 ± 4 Hz) has attracted much attention experimentally and theoretically. The synchronization of cell groups oscillating at θ frequencies in the frontal and visual cortexes has been shown to be correlated with short-term memory recall tasks [2]. θ-frequency oscillations also appear to play an important role in the encoding of spatial information by the hippocampal formation. Hippocampal place cells fire intermittent γ-frequency (25–50 Hz) bursts of action potentials when the animal is in a cell's corresponding place field, with the bursts occurring at successively earlier phases of the background hippocampal θ rhythm as the animal moves through the place field [3]. That is, in the hippocampus, the θ oscillation appears to enable the phase coding of location (while the instantaneous firing rate itself may encode speed [4]). Phase precession also allows for the spikes from multiple place cells to occur within a single θ cycle, a time range conducive for spike timing-dependent plasticity and, presumably, the consolidation of long-term memories [5].

Much of the communication between the hippocampus and the neocortex is via the entorhinal cortex (EC). Principal neurons throughout the EC receive inputs from different areas of the neocortex, and the main outputs of the EC are the perforant pathway axons of the stellate cells in layer II, which project primarily to the dentate gyrus in the hippocampal formation. The dentate gyrus projects in turn to hippocampal region CA3, which projects to CA1, which then projects back to EC layer V. The pyramidal cells in layer V project back to the neocortex as well as to layers II and III. Additionally, layer II has a large number of recurrent connections [6].

These anatomical connections make it probable that the behavior of hippocampal place cells is strongly influenced by the entorhinal cortex, and in particular by the stellate cells of layer II. Further evidence of this has come from the recent discovery of grid cells in layers II and III of the medial entorhinal cortex [7]. Grid cells are like hippocampal place cells in that they selectively fire whenever the animal is within certain spatial regions, but unlike place cells, each grid cell is associated with multiple such regions, which appear to be arranged on a triangular or hexagonal grid. In layer II, the grid spacing and orientation are similar between grid cells at the same location along the dorsoventral axis, and the relative offset between any two cells' grids is randomly distributed; the grid spacing is also known to be larger for more ventrally located grid cells [7]. Grid cells therefore appear to represent a preliminary stage to place cells in the representation and processing of spatial information. Models have been proposed to explain how place cells firing at only a single location can result from the summation of multiple grid cell inputs [8,9], as well as how the periodic grid cell firing pattern itself forms from the interference patterns of oscillatory inputs with slightly different frequencies depending on the direction of movement [10].

In the entorhinal cortex, as in the hippocampus, there is a local θ rhythm. In layer II, phase-precession effects in the firing of individual grid cells with respect to the background entorhinal θ as the animal moves through the multiple grid regions have been observed, similar to what is seen in hippocampal place cells and fields. Both the entorhinal θ rhythm and the grid cell phase precession persist even when

*Corresponding author: pcrotty@colgate.edu.

the hippocampus is inactivated or removed, suggesting that the grid cells are where the phase-precession phenomenon originates [11].

The establishment and maintenance of a stable entorhinal θ rhythm therefore appears to be a crucial component in the information processing and long-term memory consolidation performed by the entorhinal-hippocampal system. Studies of layer II stellate cells indicates that the interaction of a hyperpolarization-active cation current (h current) and a persistent sodium current can give rise to a θ-frequency subthreshold oscillation of the membrane potential in a single isolated cell [12,13]. Interestingly, the subthreshold oscillation frequency of individual stellate cells decreases in the ventral direction [14], possibly due to changes in the time constants of the h current [15]; there may therefore be a functional link between the subthreshold frequency and the grid spacing, as suggested by top-down models [10]. The large-scale entorhinal θ rhythm thus seems to be due to the synchronization of large numbers of intrinsically oscillating stellate cells that are to some degree heterogeneous in their intrinsic characteristics. However, much about the ways in which this synchronization is effected, such as the network topology, the involvement of layer II interneurons and of principal neurons in other entorhinal layers, and the extent of excitatory versus inhibitory coupling, remains comparatively unclear [16,17].

Despite these gaps in experimental knowledge about the stellate cell network, there has been considerable interest among modelers and theorists in this system since biologically realistic models first became available about ten years ago. Individual stellate cell models have been studied extensively from the point of view of dynamical systems theory [18,19], and networked stellate cell models have been used to study how synchronization is affected by parameters such as coupling strength and noise [20] and to simulate phase precession [21].

An important consideration that has been largely neglected in stellate cell synchronization studies as well as in studies of neural synchrony more generally is metabolic energy consumption. In order to function properly, neurons must consume metabolic energy to power the ATPase ion pumps that maintain ionic concentration gradients across the membrane [22,23]. These signalling-related energy costs are quite substantial, representing by far the largest proportion of metabolic energy consumed in the brain [24]. Optimizations taking energy constraints into account have proven critical to understanding the observed values of parameters such as ionic channel densities in the squid giant axon [25], mean firing frequencies [26], and quantal failure rates [27]. However, very little research has been done on the relationship of energy consumption to network properties, and the few studies that have been published have looked only at the classic Hodgkin-Huxley model [28] or at simplified, nonbiologically realistic models [29] without the intrinsic subthreshold oscillatory behavior of stellate cells.

It seems likely that metabolic energy constraints would strongly influence the optimality of the parameters that govern the synchronization of multiple neurons. Generally speaking, we might expect neurons that took longer to synchronize would consume more energy in doing so, since metabolic energy is consumed during action potentials as well as during the intervals between them. Thus, fast synchronization is likely beneficial both for its own sake and also for energetic cost. In this study, we investigate both the energy consumed during synchronization and the total time for the synchronization to occur from an initially random state.

Couplings between neurons can take the form of excitatory or inhibitory chemical synapses or direct electrical synapses, and all of these are likely to have different effects on synchronization time and energy consumption; for example, inhibitory coupling has been shown to lead to better synchronization of Hodgkin-Huxley neurons than excitatory coupling [30], while electrical coupling has been shown to be even more effective in synchronizing quadratic integrate-and-fire neurons [31].

The intrinsic oscillation frequency of the neurons could also influence the energy- and time-optimal values of the coupling and network parameters. One reason is that the relative energy costs of action potentials and quiescence depend on the spiking frequencies. Even at rest, transmembrane ionic currents still exist and lead to metabolic energy consumption. For sufficiently low frequencies, more energy is consumed during these interspike periods than by the action potentials themselves.

Finally, the network topology itself is likely to be an important factor influencing synchronization time and energy. Studies of topology and synchrony have reached a diverse range of conclusions about the optimal topology for synchronization and stability depending on the neuronal model type [32–36]. To our knowledge there have been no systematic studies of this sort thus far using stellate cell models, nor ones which explicitly consider the time for synchronization to occur or the metabolic energy consumed in doing so.

II. METHODS

A. Stellate cell model

Our monocompartmental stellate cell model is based on [20], which is itself based on the experimentally based multicompartmental model presented in Refs. [12,13]. The ionic currents in the model consist of a fast and persistent Na^+ current, a delayed-rectifier K^+ current, and a hyperpolarization-activated cation current with separate fast and slow components, as well as a leak current (assumed to be K^+). For cell i, where $1 \leqslant i \leqslant N$ and N is the total number of cells in the network, we define the membrane potential V_i to be the electric potential of the interior with respect to the extracellular medium. Since $N \leqslant 3$ in this study, we refer to these small networks alternatively as circuits. The membrane potential obeys

$$C\frac{dV_i}{dt} = I_{\mathrm{ext},i} - I_{\mathrm{Na},i} - I_{\mathrm{NaP},i} - I_{\mathrm{Kdr},i}, \\ - I_{H,i} - I_{L,i} - \sum_{j=1}^{N} I_{s,ij}, \quad (1)$$

where $I_{s,ij}$ is the synaptic current from cell j to cell i, and $I_{\mathrm{ext},i}$ is the external input current to the cell (apart from synaptic inputs). In keeping with standard conventions, $I_{\mathrm{ext},i}$ is defined to be >0 for inward (positive) current, while all the other currents are defined as negative for inward current.

The ionic currents are

$$\begin{aligned} I_{\mathrm{Na},i} &= \bar{G}_{\mathrm{Na},i} m_i^3 h_i (V_i - E_{\mathrm{Na}}), \\ I_{\mathrm{NaP},i} &= \bar{G}_{\mathrm{NaP},i} x_i (V_i - E_{\mathrm{Na}}), \\ I_{\mathrm{Kdr},i} &= \bar{G}_{\mathrm{Kdr},i} n_i (V_i - E_{\mathrm{K}}), \\ I_{H,i} &= \bar{G}_{H,i} (0.65 H_{fi} + 0.35 H_{si})(V_i - E_H), \\ I_{L,i} &= G_{L,i} (V_i - E_{\mathrm{K}}). \end{aligned} \tag{2}$$

Note the approximately 2:1 ratio between the fast (H_f) and slow (H_s) components of the h current, which is based on experimental recordings [12].

The ionic current state variables obey

$$\frac{ds_i}{dt} = \frac{s_\infty(V_i) - s_i}{\tau_s(V_i)} = \alpha_s(V_i)(1 - s_i) - \beta_s(V_i) s_i, \tag{3}$$

where $s = m, h, x, n, H_f$, or H_s, and

$$s_\infty = \alpha_s / (\alpha_s + \beta_s), \tag{4}$$

$$\tau_s = 1/(\alpha_s + \beta_s). \tag{5}$$

The kinetic rate coefficients α_s and β_s are functions of voltage. Empirical results fits are given in, e.g., [20].

The synaptic currents are

$$I_{s,ij} = \bar{G}_{s,ij} z_{ij} (V_i - E_{s,ij}). \tag{6}$$

We allow for the connection strength ($\bar{G}_{s,ij}$) and the synaptic reversal potential ($E_{s,ij}$) to vary for each synapse. By definition, excitatory chemical synapses have a value of $E_{s,ij}$ above (more depolarized than) the firing threshold, and inhibitory ones have a value of $E_{s,ij}$ beneath it.

The stellate cell model was implemented using NEURON/NMODL [37], supplemented by parameter-sweeping software written in PYTHON. The simulations were performed on a 26-CPU Beowulf cluster running Gentoo Linux and used a 25-μs time step. MATLAB was used for plotting and numerical analysis.

B. Synchronization

Although precise mathematical measures of synchronization such as the Kuramoto order parameter [38] exist for populations of relatively simple oscillators with explicit phase variables, more general definitions for highly nontrivial oscillators like biologically realistic neurons are somewhat elusive in the literature. We can clearly call a group of neurons synchronized if they all fire at the same times, but it is less clear how to characterize their degree of synchronization when they do not. There are many ways to define a phase difference; the simplest is just to use the time difference between spikes modulo the period. Thus, two regularly spiking neurons with period T can be said to have a phase difference of $T/2$ if their action potentials are half a period apart. Groups of three or more neurons can have their synchronization quantified by, e.g., the sample standard deviation of their phases. Phases for off-limit cycle neurons can be defined by "isochrons," subspaces of the dynamical system state space from which trajectories asymptotically go to the same point on the limit cycle as an on-cycle point at a certain phase [39]. However, calculating isochrons in all but the simplest cases is computationally extremely intensive, particularly for high-dimensional systems. More generally, there is no reason to prefer one measure of synchronization to another unless the biological relevance of the measure is apparent. In the brain, the local field potential is what is usually measured experimentally, but predicting the LFP from the individual activity of nearby neurons remains a largely unsolved problem [40].

We adopt a somewhat different approach here and calculate the mean time it takes a group of neurons to synchronize their firing from an initially random distribution of phases. Synchronization is defined to have occurred when all of the action potential peaks are within one action potential width, approximately 3 ms, of each other. The mean synchronization time T_{sync} is averaged over a representative sample of initial phase conditions. For the two-neuron results below, T_{sync} was averaged over 200 evenly spaced initial phase differences between the neurons from $-T/2$ to $+T/2$. For three and more neurons, because of computational time constraints, we used a Monte Carlo approach and randomly selected 200 initial phase conditions assuming uniform distributions for all the phases. We verified for several representative cases that our calculated values of T_{sync} were not significantly changed by rerunning the simulations with different random phases, by increasing the number of phase points to 1000, or by decreasing the simulation time step from 25 to 5 μs. The statistical fluctuations due to the random sampling are of order a few percent and account for the slightly bumpy appearance of Figs. 8–11.

The metabolic energy consumed during synchronization is due to the ATPase Na^+/K^+ ionic pump in the neuronal membrane, which must restore the resting ionic concentration gradients after a period of electrical activity. The energy cost is proportional to the number of Na^+ ions which cross the membrane and can be calculated by integrating the Na^+ current [41]. For the purposes of this study, we assume that the h current and leak current are comprised of separate Na^+ and K^+ channels with the same kinetics. While cells consume metabolic energy regardless of whether or not they are coupled or synchronized, since we are interested in the energy cost specifically associated with synchronization, we begin counting energy consumption only from the onset of synaptic coupling (the dashed vertical lines in Figs. 1 and 2).

C. Topology

The neuronal circuits simulated here consist of two or three identical stellate cells connected by excitatory or inhibitory synapses (see Table I). Excitatory synapses have a reversal potential of $E_{s,ij} = 0$ mV, and inhibitory synapses have $E_{s,ij} = -50$ mV. We verified that our main qualitative results were generally insensitive to the exact value of $E_{s,ij}$. All of the synapses in a circuit have the same weight, represented by the synaptic conductance $\bar{G}_s$.

We excluded network topologies with self-connected neurons and/or completely isolated neurons lacking either incoming or outgoing synaptic connections. For two identical neurons and a given value of $\bar{G}_s$, there are then five qualitatively distinct connection topologies: mutual excitatory connections, mutual inhibitory connections, one excitatory and one inhibitory connection, and one neuron driving the other via an excitatory or inhibitory connection without any feedback. We simulated all of these circuits. For three neurons, there are

TABLE I. Unless otherwise specified, the following parameter values, which are based on experimental measurements, were used in the stellate cell model. Note that the model is isopotential. The value of the membrane capacitance C includes gating capacitances. The conductance values are the maximal possible ones (i.e., with all channels open).

Symbol	Meaning	Value/Units
A	surface area	$1000\,\mu\text{m}^2$
C	membrane capacitance	$1.5\,\mu\text{F/cm}^2$
$\bar{G}_{\text{Na}}$	fast Na^+ conductance	$52\,\text{mS/cm}^2$
$\bar{G}_{\text{Kdr}}$	K^+ conductance	$11\,\text{mS/cm}^2$
G_L	leak conductance	$0.5\,\text{mS/cm}^2$
$\bar{G}_H$	h conductance	$1.5\,\text{mS/cm}^2$
$\bar{G}_{\text{NaP}}$	persistent Na^+ conductance	$0.5\,\text{mS/cm}^2$
$\bar{G}_s$	synaptic conductance	$0.01\,\text{mS/cm}^2$
E_{Na}	Na^+ reversal potential	55 mV
E_{K}	K^+ reversal potential	-90 mV
E_L	leak reversal potential	-65 mV
E_H	h-current reversal potential	-20 mV
E_s	synaptic reversal potential	0 (excit) mV -50 (inhib)
I_{ext}	external bias current	$-0.00225\,\text{mA/cm}^2$

78 distinct network topologies. We simulated the ten of these topologies that are fully recurrent, meaning that every neuron has both incoming and outgoing connections, and are also synaptically uniform in that all synapses in the circuit are either excitatory or inhibitory (in line with experimental observations that a given neuronal type only makes one or the other). We also simulated several additional three-neuron circuits in which the synapse types were mixed and/or one neuron made only presynaptic connections with the others, in which case it could be considered as "driving" the synchronization.

III. RESULTS

Figures 1 and 2 are examples of the simulations on which our results are based. Stellate cell neurons with given values for the persistent sodium conductance $\bar{G}_{\text{NaP}}$ and the h-current conductance $\bar{G}_H$ and initially firing out of phase with each other have mutual synaptic coupling turned at a time represented by the dashed vertical line. Then, the simulated time that it takes for their firings to synchronize to within one action potential width (about 3 ms) is calculated. We also calculate the total metabolic energy consumed during the synchronization process.

The h current and persistent sodium conductances have a strong effect on the intrinsic firing frequency of an isolated stellate cell (SC) neuron, as shown in Fig. 3. The frequency increases monotonically with both $\bar{G}_{\text{NaP}}$ and $\bar{G}_H$, rising by a factor of nearly 10 for a twofold increase in both. Of the other three membrane ionic conductances, only the leak conductance G_L has an effect of similar magnitude on the frequency. (We did not systematically vary G_L because it is restricted to a much smaller range: above about 0.5 mS/cm^2, the neuron stops firing.)

Our goal was to determine whether certain values for $\bar{G}_{\text{NaP}}$ and $\bar{G}_H$ are better than others for the time and energy costs

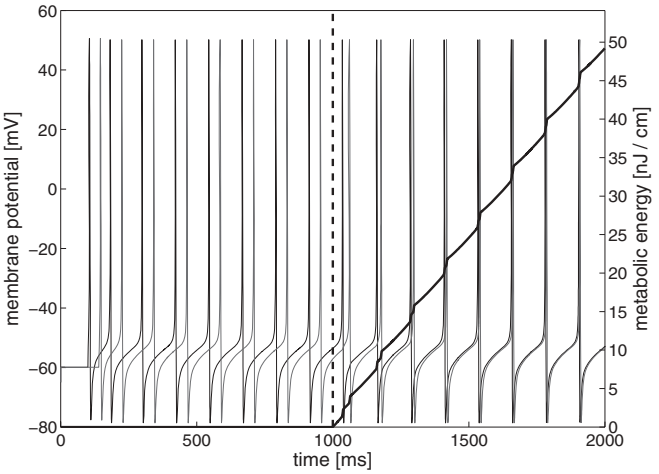

FIG. 1. Two identical stellate cells with intrinsic 8-Hz firing frequencies are initially one-third of a period (40 ms) out of phase. At $t = 1000$ ms, mutual excitatory coupling is turned on, and the cells synchronize to within 1 action potential width (3 ms) by about $t = 1900$ ms. The amounts of metabolic energy (solid black line) consumed during action potentials and interspike intervals are fairly similar. We only calculate metabolic energy consumption from the onset of synaptic coupling, although each cell individually consumes energy before the coupling is turned on. The brief higher-frequency spiking at the beginning is an initial transient.

of synchronization. The most general assumption about the initial phases of the cells before synaptic coupling is turned on is that they are randomly distributed. Therefore, for each circuit configuration (number of cells N, circuit topology, and synaptic strength $\bar{G}_s$) and each pair of $\bar{G}_{\text{NaP}}$ and $\bar{G}_H$ values, we averaged T_{sync} and U_{sync} over the different possible sets of initial phases, assuming a uniform distribution (see Sec. II B).

In Figs. 4 and 5, we show a typical result. In this case, for two neurons with mutual excitatory synaptic coupling with $\bar{G}_s = 0.01\,\text{mS/cm}^2$, the mean synchronization time as a function of $\bar{G}_{\text{NaP}}$ and $\bar{G}_H$ has a conspicuous "valley" of minima in which T_{sync} is several times lower than it is for nearby $(\bar{G}_H, \bar{G}_{\text{NaP}})$

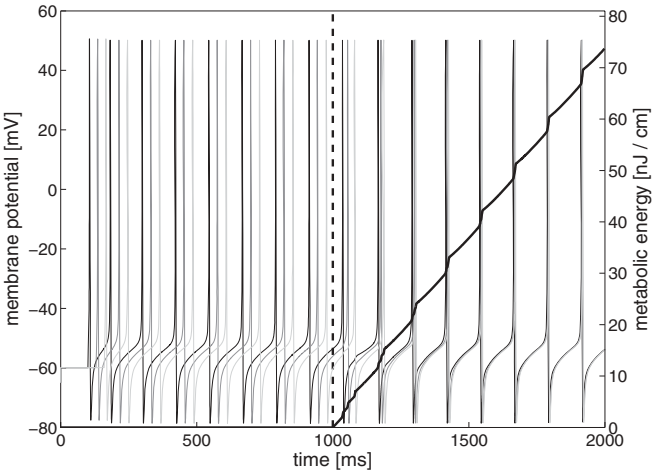

FIG. 2. Three identical 8 Hz cells are initially out of phase by 20 ms increments. All-to-all excitatory coupling is turned on at $t = 1000$ ms.

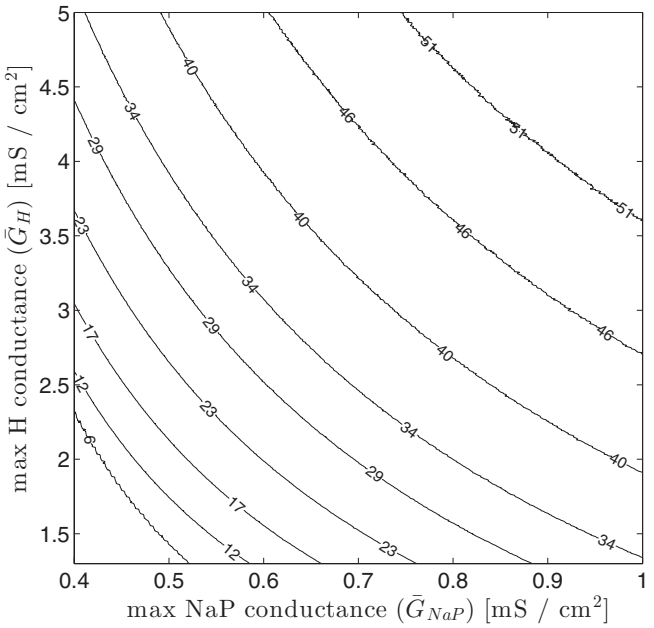

FIG. 3. The intrinsic spiking frequency (f, in Hz) of stellate cell neurons is strongly influenced by the channel densities or maximum conductances of the persistent sodium current ($\bar{G}_{\mathrm{NaP}}$) and h current ($\bar{G}_H$). In the region below the bottom left contour, the neuron does not fire (i.e., frequency goes to 0).

values. We show a top-down view of the T_{sync} surface in Fig. 5. The T_{sync} minima, shown by dots, lie very close to the

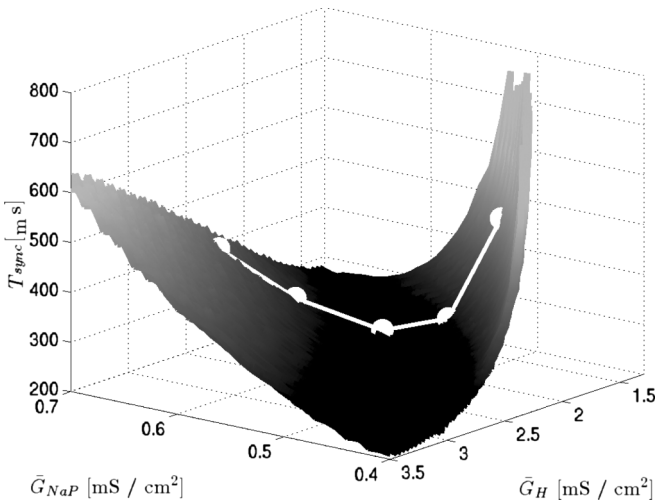

FIG. 4. The mean time for two symmetrically coupled neurons with random initial phases to synchronize to within one action potential width (T_{sync}) is shown as a function of $\bar{G}_H$ and $\bar{G}_{\mathrm{NaP}}$. There is a valley of minima around the 20-Hz isofrequency contour. Here and in all subsequent figures of this type, the synaptic conductance is $\bar{G}_s = 0.01$ mS/cm^2, but the existence and locations of valleys of minima are largely independent of the value of $\bar{G}_s$ over the range $0.006 \leqslant \bar{G}_s \leqslant 0.06$ mS/cm^2. Darker shades of grey correspond to lower values of T_{sync}, i.e., faster synchronization. The resolution for both $\bar{G}_H$ and $\bar{G}_{\mathrm{NaP}}$ is 0.01 mS/cm^2. The embedded line and circles show the points considered for the phase response curve calculations in Figs. 13 and 14.

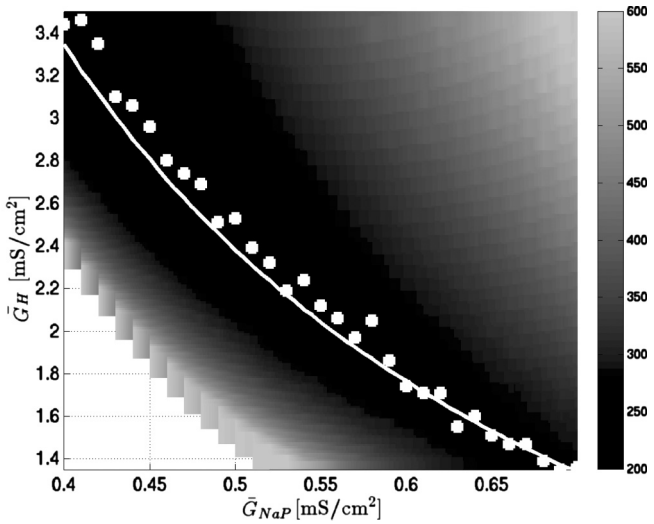

FIG. 5. Top-down view of the surface in Fig. 4. The color bar shows the value of T_{sync} in ms. The valley bottom, i.e., the points at which T_{sync} is lowest for each value of $\bar{G}_{\mathrm{NaP}}$ (and which are colored the darkest), is shown by dots (•). The solid line is the 20-Hz isofrequency contour. At the lower left edge, corresponding to the right side of the surface in Fig. 4, T_{sync} rises sharply. Below this boundary, the neurons do not fire repetitively.

20-Hz isofrequency contour, shown by a solid line. (The slight jaggedness in these and other curves is due to the plotting and simulation resolutions.) The energy of synchronization, U_{sync}, also has a valley of minima at roughly the same place (Fig. 6).

This optimal region of $(\bar{G}_H, \bar{G}_{\mathrm{NaP}})$ parameter space for T_{sync} and U_{sync} persists in approximately the same place for values of $\bar{G}_s$ ranging from about 0.006 to 0.06 mS/cm^2, although the actual values for the synchronization time and energy at any given $(\bar{G}_H, \bar{G}_{\mathrm{NaP}})$ point decrease with increasing synaptic strength by a factor of about 10 over that range. The low-frequency valley also persists when the mutual coupling between two neurons is inhibitory rather than excitatory, as shown in Fig. 7. For inhibitory coupling, we used a synaptic

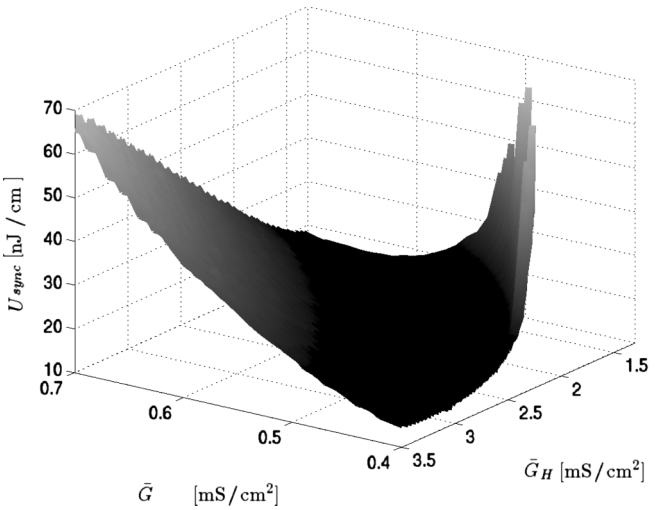

FIG. 6. The mean energy consumed during synchronization for the two neurons in Fig. 4 also has a valley of minima near the one for T_{sync}.

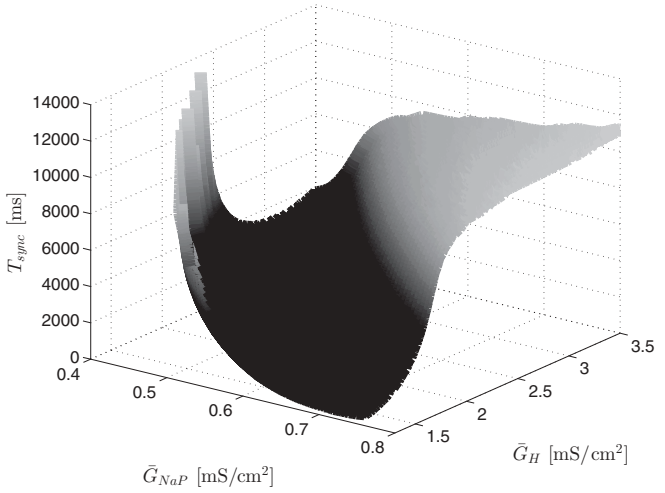

FIG. 7. Although it takes significantly longer for two neurons to synchronize when they are connected with inhibitory synapses, the valley of minima at low frequencies persists.

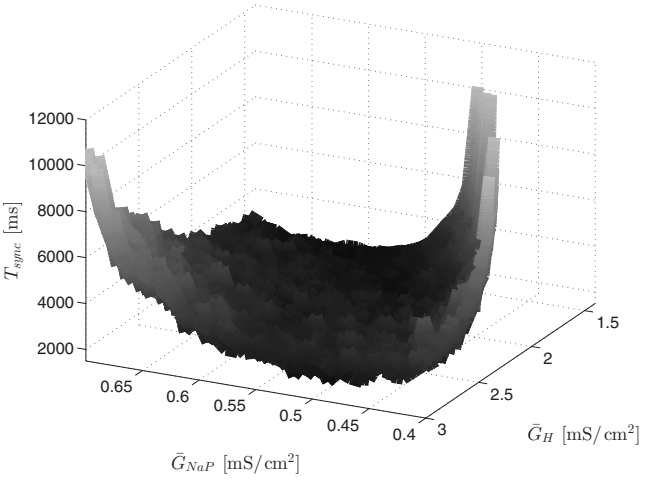

FIG. 9. As in the two-neuron case, the overall synchronization time scale is substantially larger when three neurons are connected with all-to-all inhibitory coupling, but the valley of minima is still present.

reversal potential of $E_s = -50$ mV, but we verified that the location of the valley is relatively insensitive to E_s in the range $-70 \leqslant E_s \leqslant -30$ mV. The value of the synaptic conductance $\bar{G}_s$ in Fig. 7 and in all subsequent surface-plot figures is 0.01 mS/cm^2.

Valleys of minima are present in many cases for three coupled neurons. In Fig. 8, we show T_{sync} as a function of $\bar{G}_H$ and $\bar{G}_{\text{NaP}}$ for three identical neurons with all-to-all excitatory coupling (that is, every neuron has an excitatory synapse on every other neuron). A valley also exists for inhibitory all-to-all coupling (Fig. 9) and for cyclic excitatory coupling, in which neuron 1 is connected to neuron 2, which is connected to neuron 3, which is connected back to neuron 1 (Fig. 10).

We simulated all of the ten nontrivial, fully connected circuit topologies for three identical neurons connected with excitatory or inhibitory synapses (but not both) of the same strength ($\bar{G}_s$), and we simulated a cyclic circuit with excitatory connections in one direction and inhibitory connections in the other. Additionally, we simulated eight topologies in which one neuron drives the other two via excitatory or inhibitory connections; the other two neurons may also be connected to each other. We found in general that the valleys of minima are present for the first 11 circuits and the excitatory-inhibitory cyclic circuit, but not for the eight circuits in which one neuron drives the other two. The major difference between the two groups of topologies is that the first 11 are recurrent: a path of synaptic connections exists from each neuron back to itself. The latter eight are feed-forward topologies in which one neuron has a one-way connection to the others. Even though these circuits also synchronize (Fig. 11), the low-frequency range is not especially favored for synchronization time or energy.

In Fig. 12, we show the locations of points along the valleys of minima for several different topologies with $N = 2$ and $N = 3$. While the valley bottoms are not all in the same place, they

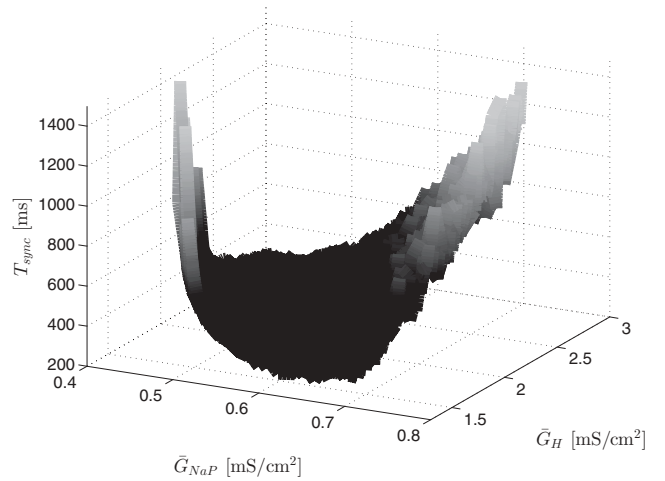

FIG. 8. The valley of minima is present for three neurons with excitatory all-to-all coupling. The slight bumpiness here and in Figs. 9–11 is due to the Monte Carlo phase-sampling technique used for three-neuron circuits (see Sec. II B).

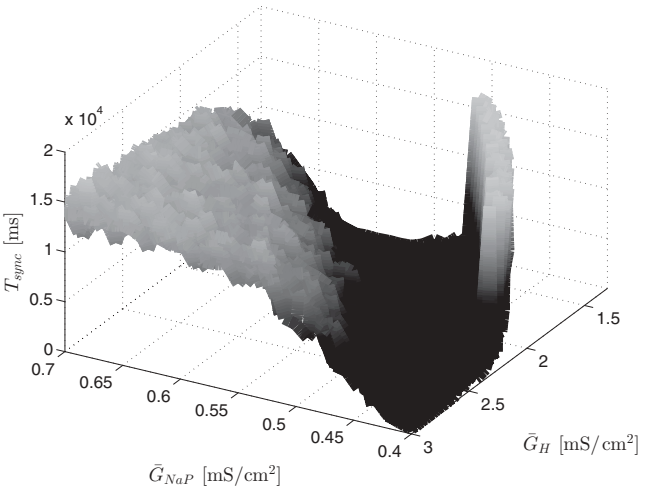

FIG. 10. Minima exist for the synchronization time for three neurons with cyclic excitatory coupling, and for recurrently connected three-cell circuits in general.

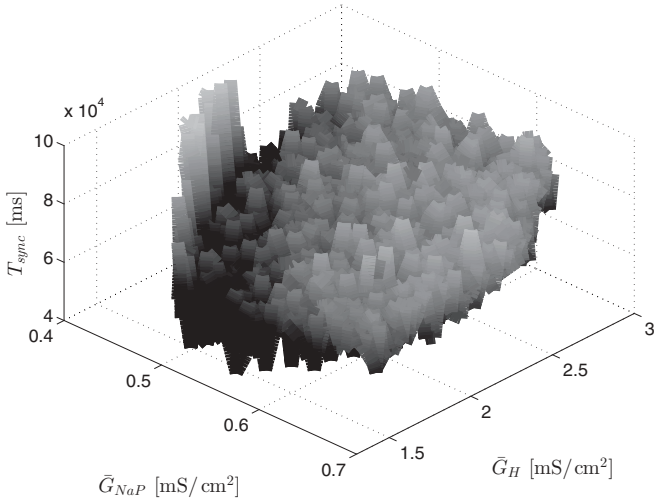

FIG. 11. The valley of minima almost disappears when one neuron is connected to the other two via excitatory connections without any feedback, although synchronization does eventually occur. The synchronization time and metabolic energy costs are also larger than they are for cyclic or all-to-all connections by at least an order of magnitude. This absence of regions of significant minima and very long synchronization times is a general feature of feed-forward circuit topologies for three neurons.

are all in the low-frequency range. In most cases, the valleys are broad enough to substantially include the 8–12-Hz θ firing frequency range actually observed for stellate cell neurons.

Mathematically, the existence of a region of minima for T_{sync} and U_{sync} is a phenomenon of the system of highly nonlinear coupled differential equations [Eqs. (2)–(6)] describing the stellate cells. While a fully analytical derivation of the valleys of minima is probably impossible, some insight can be gained from considering the phase response curves (PRCs) for the

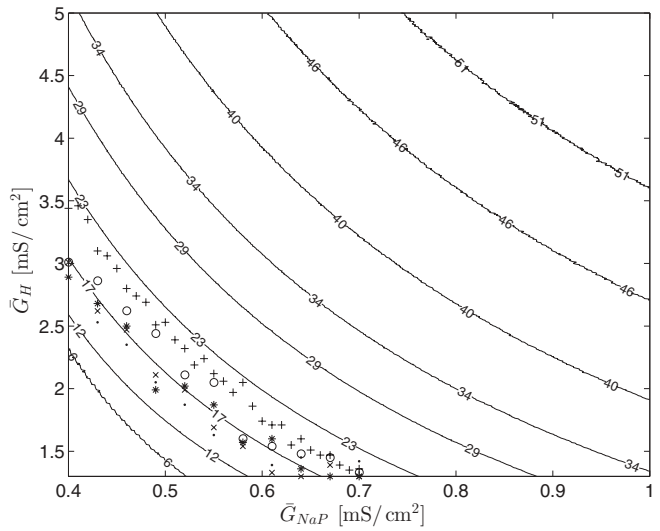

FIG. 12. Locations of the T_{sync} minima for different two- and three-neuron circuit topologies. +: $N = 2$, all-to-all excitatory; ○: $N = 3$, all-to-all excitatory; ∗: $N = 3$, all-to-all inhibitory; ·: $N = 3$, cyclic excitatory; ×: $N = 3$, cyclic with excitatory connections in one direction and inhibitory connections in the other. In all cases, $\bar{G}_s = 0.01$ mS/cm^2.

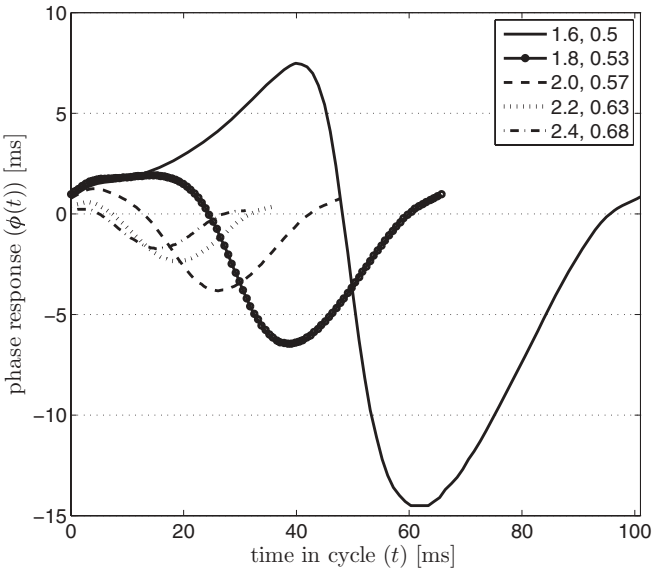

FIG. 13. The phase response curve [$\phi(t)$] gives the change in phase for an oscillating neuron in response to an input stimulus of given duration and size at a time t within the neuron's natural cycle. The next action potential is shifted in time by ϕ from when it would have been without the input stimulus; thus, negative values of ϕ mean that the action potential occurs sooner. The figure shows $\phi(t)$ versus t for five different ($\bar{G}_H$, $\bar{G}_{\text{NaP}}$) (mS/cm^2) points on both sides of the valley of minima; the (2.0, 0.57) mS/cm^2 point is approximately at the bottom. The input is an excitatory synaptic stimulus with $\bar{G}_s = 0.01$ mS/cm^2. The phase response does not go to 0 exactly at $t = 0$ because of the finite width of the input pulse. The frequency increases as one moves to the "far" side of the valley (higher values of the conductances), and thus the period is shorter.

cells. A phase response curve gives the change in phase of an oscillator for an input of given strength and duration [39,42]. In Fig. 13, we show the phase response curve for a single stellate cell subject to an excitatory input pulse with $\bar{G}_s = 0.01$ mS/cm^2, choosing the five pairs of ($\bar{G}_H$,$\bar{G}_{\text{NaP}}$) values shown in Fig. 4—that is, we go "down" one side of the valley and "up" the other, with the central (2, 0.57) mS/cm^2 point approximately at the bottom.

We see from Fig. 13 that the mean size of the PRC decreases significantly as one moves from lower to higher values of the conductances. There is no obvious feature of the (2, 0.57) mS/cm^2 PRC to indicate that it is at a minimum for T_{sync}. Indeed, one might expect that the (1.6, 0.5) mS/cm^2 point would correspond to the most quickly synchronizing neurons since the typical phase change for each input pulse is largest. However, what matters for T_{sync} is not the mean phase change per input pulse but the mean phase change per unit time. The neurons with smaller average PRCs also spike more frequently, and therefore we might expect a tradeoff between the mean phase change and the spiking frequency. In Fig. 14, we plot the mean phase change divided by the oscillation period. This quantity, the mean amount by which the phase changes per unit time, is largest for the central point near the valley bottom (negative values indicate that the action potentials are stimulated to happen before they would have otherwise). That is, we can associate each phase response curve with a rate of synchronization, which is fastest in the valleys.

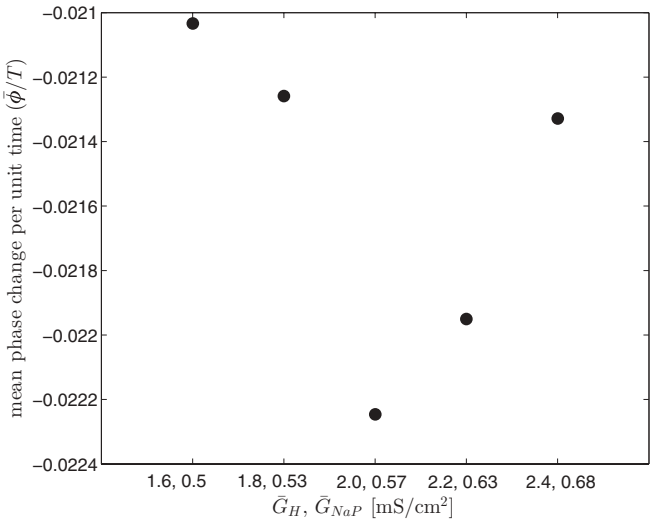

FIG. 14. The mean value of ϕ ($\bar{\phi}$) divided by the period (T) is shown for the five different ($\bar{G}_H$,$\bar{G}_{\mathrm{NaP}}$) values of Fig. 13. The maximum (negative) value of $\bar{\phi}/T$ is at the bottom of the valley of minima.

IV. DISCUSSION

The existence of a conspicuous valley of minima in ($\bar{G}_H$,$\bar{G}_{\mathrm{NaP}}$) phase space for mean synchronization time and metabolic energy consumption during synchronization appears to be a fairly robust feature of coupled entorhinal cortex layer II stellate cells (Fig. 12), at least in the two- and three-cell circuits we studied. In all the cases in which the valleys of minima appear, they are at low frequencies and generally cover the 10–20-Hz range. Notably, we observed no cases in which minima were apparent at higher frequencies such as the 25–50-Hz γ range. The exact values of the minima are ultimately dependent on the computational stellate cell model and the experimental data on which it is based, and many ion channel parameters remain estimates or guesswork based on fits to the data. It it is quite possible that the few-Hz discrepancy between the minima and the θ range would decrease or disappear with a more accurate computational model. Nevertheless, even with these limitations, it is still remarkable that the model strongly predicts that stellate cells with intrinsic firing frequencies of about 10–20 Hz synchronize their firing much faster, and require much less metabolic energy consumption to do so, than stellate cells with firing frequencies that are significantly higher or lower.

These results persist over an order of magnitude of synaptic coupling strength ($0.006 \leqslant \bar{G}_s \leqslant 0.06$ mS/cm^2) and are generally insensitive to the value of the synaptic reversal potential (E_s) apart from its being excitatory or inhibitory. The only important factor governing the existence of a valley of minima appears to be the network topology: for circuits of two or three neurons with recurrent topologies, significant valleys are present, but they are extremely weak or nonexistent for feed-forward topologies in which one of the neurons drives the others without any synaptic connections back from them, even though synchronization does eventually occur. In general, the circuits synchronize faster for excitatory versus inhibitory coupling and for all-to-all versus cyclic topologies, while the feed-forward circuits are the slowest of all.

Overall, the observed values of $\bar{G}_H$ and $\bar{G}_{\mathrm{NaP}}$, and accordingly the experimentally observed low-frequency firing of the stellate cells, are in the range advantageous for quick synchronization time and minimal metabolic energy costs during synchronization. The network topology also plays a strong role, and while the detailed anatomy of the entorhinal cortex remains poorly understood, the connections between the stellate cells are known to be recurrent. Provided that the topology allows for it, the phase response curves and firing frequencies can be used to determine approximately where the minima of T_{sync} are.

More generally, our results may provide some insight into why the sustained oscillations seen in the brain tend to be lower frequency. While γ frequency oscillations and hippocampal "ripple" oscillations with frequencies of up to 200 Hz can be measured in hippocampal LFPs, higher-frequency oscillations generally do not last for longer than a tenth of a second. The sustained oscillations seen in the neocortex as well as the hippocampus, for example during memory recall tasks [2], are generally in the θ range. If the same dynamics are operative among the cells of these other areas, lower frequencies might also be optimal for their synchronization time and energy consumption.

Because of computational constraints, we have looked only at small networks of identical neurons, and further research will focus on more realistic scenarios such as larger numbers of cells with more complex topologies, heterogeneous distributions of intrinsic firing frequencies and synaptic weights, the presence of channel noise, and external inputs. There are also considerations such as synaptic plasticity, physical volume constraints, energetic and temporal costs associated with wiring and cell morphology, etc., that could affect optimizations and which merit future study. Nevertheless, the possibility exists that the observed firing frequencies of stellate cells and of other central neurons reflect evolutionary pressures towards fast synchronization for low metabolic energy cost. What is important for central neurons is not only the existence of stable synchronization states, but also the time and energy necessary to achieve them.

ACKNOWLEDGMENTS

We thank T. Sangrey and M. Yoshida for useful discussions. This work was supported by Grant No. SFB 874, Project B2, from the German Research Foundation (Deutsche Forschungsgemeinschaft, DFG) and a grant from the Stiftung Mercator to S.C.

[1] G. Buzsaki, Hippocampus **15**, 827 (2005).
[2] S. Liebe, G. M. Hoerzer, N. K. Logothetis, and G. Rainer, Nat. Neurosci. **15**, 456 (2012).
[3] J. O'Keefe and M. L. Recce, Hippocampus **3**, 317 (1993).
[4] J. Huxter, N. Burgess, and J. O'Keefe, Nature (London) **425**, 828 (2003).

[5] G. Dragoi and G. Buzsaki, Neuron **50**, 145 (2006).
[6] *The Hippocampus Book*, 1st ed., edited by P. Andersen, R. Morris, D. Amaral, T. Bliss, and J. O'Keefe (Oxford University Press, Oxford, UK, 2006).
[7] T. Hafting, M. Fyhn, S. Molden, M.-B. Moser, and E. I. Moser, Nature (London) **436**, 801 (2005).
[8] T. Solstad, E. I. Moser, and G. T. Einevoll, Hippocampus **16**, 1026 (2006).
[9] S. Cheng and L. M. Frank, Neuroscience **197**, 293 (2011).
[10] N. Burgess, C. Barry, and J. O'Keefe, Hippocampus **17**, 801 (2007).
[11] T. Hafting, M. Fyhn, T. Bonnevie, M.-B. Moser, and E. I. Moser, Nature (London) **453**, 1248 (2008).
[12] C. T. Dickson, J. Magistretti, M. H. Shalinsky, E. Fransen, M. E. Hasselmo, and A. Alonso, J. Neurophysiol. **83**, 2562 (2000).
[13] E. Fransen, A. Alonso, C. Dickson, J. Magistretti, and M. Hasselmo, Hippocampus **14**, 368 (2004).
[14] L. M. Giocomo, E. A. Zilli, E. Fransen, and M. E. Hasselmo, Science **315**, 1719 (2007).
[15] L. M. Giocomo and M. E. Hasselmo, J. Neurosci. **28**, 9414 (2008).
[16] C. B. Canto, F. G. Wouterlood, and M. P. Witter, Neural Plast. **2008**, 381243 (2008).
[17] S. S. Kumar and P. S. Buckmaster, J. Neurosci. **26**, 4613 (2006).
[18] H. G. Rotstein, T. Oppermann, J. A. White, and N. Kopell, J. Comput. Neurosci. **21**, 271 (2006).
[19] T. Kispersky, J. A. White, and H. G. Rotstein, PLoS ONE **5**, e13697 (2010).
[20] C. D. Acker, N. Kopell, and J. A. White, J. Comput. Neurosci. **15**, 71 (2003).
[21] J. Igarashi, H. Hayashi, and K. Tateno, Cognit. Neurodyn. **1**, 169 (2007).
[22] B. Hille, *Ion Channels of Excitable Membranes* (Sinauer Associates, Sunderland, MA, 2001).
[23] T. F. Weiss, *Cellular Biophysics* (MIT Press, Cambridge, MA, 1996).
[24] D. Attwell and S. B. Laughlin, J. Cereb. Blood Flow Metab. **21**, 1133 (2001).
[25] P. Crotty, T. D. Sangrey, and W. B. Levy, J. Neurophysiol. **96**, 1237 (2006).
[26] W. B. Levy and R. A. Baxter, Neural Comput. **8**, 531 (1996).
[27] W. B. Levy and R. A. Baxter, J. Neurosci. **22**, 4746 (2002).
[28] A. Moujahid, A. d'Anjou, F. J. Torrealdea, and F. Torrealdea, Phys. Rev. E **83**, 031912 (2011).
[29] F. J. Torrealdea, A. d'Anjou, M. Grana, and C. Sarasola, Phys. Rev. E **74**, 011905 (2006).
[30] C. van Vreeswijk and L. F. Abbott, J. Comput. Neurosci. **1**, 313 (1994).
[31] N. Kopell and B. Ermentrout, Proc. Natl. Acad. Sci. **101**, 15482 (2004).
[32] O. Kwon and H.-T. Moon, Phys. Lett. A **298**, 319 (2002).
[33] I. Belykh, E. de Lange, and M. Hasler, Phys. Rev. Lett. **94**, 188101 (2005).
[34] L. Fortuna, M. Frasca, M. L. Rosa, and A. Spata, Chaos **15**, 014102 (2005).
[35] D. Eytan and S. Marom, J. Neurosci. **26**, 8465 (2006).
[36] Y. Gao and J. Wang, Phys. Rev. E **83**, 031909 (2011).
[37] M. L. Hines and N. T. Carnevale, Neural Comput. **9**, 1179 (1997).
[38] S. H. Strogatz, Physica D **143**, 1 (2000).
[39] E. M. Izhikevich, *Dynamical Systems in Neuroscience: The Geometry of Excitability and Bursting* (MIT Press, Cambridge, MA, 2007).
[40] J. N. Milstein and C. Koch, Neural Comput. **20**, 2070 (2008).
[41] P. Crotty and T. Sangrey, Neurocomputing **74**, 3843 (2011).
[42] R. M. Smeal, G. B. Ermentrout, and J. A. White, Philos. Trans. R. Soc. B **365**, 2407 (2010).